Continental Shelf Research 77 (2014) 51–60

Contents lists available at ScienceDirect

Continental Shelf Research

journal homepage: www.elsevier.com/locate/csr

Research papers

High frequency variability of particle size distribution and its dependency on turbulence over the sea bottom during re-suspension processes

P.R. Renosh [a], François G. Schmitt [a,*], Hubert Loisel [b], Alexei Sentchev [b], Xavier Mériaux [b]

[a] CNRS, University of Lille-1, Laboratory of Oceanology and Geosciences, CNRS UMR 8187 LOG, 32 Avenue Foch, 62930 Wimereux, France
[b] ULCO, Laboratory of Oceanology and Geosciences, UMR 8187 LOG, 32 Avenue Foch, 62930 Wimereux, France

ARTICLE INFO

Article history:
Received 22 August 2013
Received in revised form
21 January 2014
Accepted 27 January 2014
Available online 5 February 2014

Keywords:
Particle size distribution
Turbulence
Spectral analysis
Stokes number
Re-suspension processes

ABSTRACT

The impact of tidal current, waves and turbulence on particles re-suspension over the sea bottom is studied through Eulerian high frequency measurements of velocity and particle size distribution (*PSD*) during 5 tidal cycles (65 h) in a coastal environment of the eastern English Channel. High frequency variability of *PSD* is observed along with the velocity fluctuations. Power spectral analysis shows that turbulent velocity and *PSD* parameters have similarities in their spectral behaviour over the whole range of examined temporal scales. The low frequency variability of particles is controlled by turbulence ($\beta \simeq -5/3$) and the high frequency is partly driven by dynamical processes impacted by the sea bottom interactions with turbulence (wall turbulence). Stokes number (*St*), rarely measured in situ, exhibits very low values, emphasizing that these particles can be considered as passive tracers. The effect of tide and waves on turbidity and *PSD* is highlighted. During slack tide, when the current reaches its minimum value, we observe a higher proportion of small particles compared to larger ones. To a lower extent, high significant wave heights are also associated with a greater concentration of suspended sediments and the presence of larger particles (larger Sauter's diameter D_A, and lower *PSD* slope ξ).

1. Introduction

Marine particles cover a broad range in diameters from nanometers, mainly as colloids, to few millimeters and even centimeters in the presence of big *Phaeocystis* colonies, diatoms chains, or cyanobacteria filaments. Intermediate size particles include viruses, heterotrophic bacteria, pico-, nano-, and micro-, phytoplankton, micro-, meso-, and macro-zooplankton, non-living particles, and mineral particles (Stramski et al., 2004). These particles do not solely appear as individual entities in the water column, but are mainly present as marine algal flocs and aggregates (Eisma, 1986; Fowler and Knauer, 1986; Hill, 1998; Boss et al., 2009). The variability of the marine particle size distribution (*PSD*) impacts the different biological processes occurring in oceanic waters and vice versa. For instance, trophic interactions are tightly linked to the size distribution of the different living and non-living particles involved all over the trophic system (McCave, 1984). In the other way, blooms of specific phytoplankton species modify the general *PSD* shape by affecting one given size class. Phytoplankton degradation processes as well as zooplankton grazing also affect the *PSD* shape by promoting the small particles size classes compared to larger ones. Physical processes occurring in the water column are also related to the *PSD*. For example, the settling velocity of the suspended matters is strongly controlled by the particles size. In contrast, the size distribution of floc or aggregate depends on the balance between aggregation and breakage, two processes driven by diffusive turbulent transport and differential settling (McCave, 1984). McCave suggested that particles in the Brownian range ($<1.0\ \mu$m) are pumped rapidly into larger size classes by aggregation. The instantaneous turbulent kinetic energy modifies the proportion between particles/floccule, fine, coarse, microflocs and macroflocs (Lefebvre et al., 2012). The re-suspension of marine sediments is also strongly size dependent (Wells and Goldberg, 1992; Mikkelsen and Pejrup, 2001; Fettweis et al., 2006).

Turbulence is one of the most important physical phenomena which determines the re-suspension and the settling of the suspended particles in the coastal as well as oceanic waters (Eisma, 1986; Van Leussen, 1988; Umlauf and Burchard, 2005; Fettweis et al., 2006; Burchard et al., 2008; Van der Lee et al., 2009). For instance, observations on floc in the field show that smaller flocs occur in high energy environments (Kranck and Milligan, 1992; Berhane et al., 1997). At a critical magnitude of turbulence, shear overcomes the binding strength of flocs and tends to destroy aggregates (Eisma, 1986). For primary (disaggregated) particles significantly larger than $1.0\ \mu$m, and for the process of smaller flocs (microflocs) growing into larger flocs (macroflocs), turbulent shear is thought to be the dominant

* Corresponding author.
E-mail addresses: pr.renosh@gmail.com (P.R. Renosh), francois.schmitt@univ-lille1.fr (F.G. Schmitt).

http://dx.doi.org/10.1016/j.csr.2014.01.024
0278-4343

collision mechanism, except during periods of slack current velocities when differential settling of suspended particles onto one another may be responsible for most of the flocs formation and rapid clearing of the water (Van Leussen, 1988).

Studies done by Wolanski and Gibbs (1995) in Fly River Estuary show that the mean floc size was affected by the turbulence of tidal currents. The largest floc sizes were observed in the low tidal currents (<0.5 m/s) and comparatively smaller floc sizes were observed in the high tidal currents (>0.5 m/s).

In the present study, we analyse the dynamics of *PSD* and its relation with turbulence from in situ measurements. We conducted simultaneous measurements of velocity and *PSD* from instruments fixed on a frame positioned on the sea floor in the coastal waters of eastern English Channel. This study area, characterized by low depth, exhibits a large range of variability of bio-optical properties related to the occurrence of different phytoplankton blooms, bottom sediments re-suspension confined in the coastal areas, and numerous river inputs (Velegrakis et al., 1999; Loisel et al., 2007; Vantrepotte et al., 2007). The study carried out by Velegrakis et al. (1999) showed that re-suspension of fine-grained particles takes place during the spring tides and correlates well with the distribution of the bottom lithological type. In this paper, we will assess whether the re-suspended particles are passive tracers, or have an inertia that influences their transport by turbulence. For this, we estimate from in situ measurements their Stokes number *St*, which is a dimensionless number explaining the effect of inertia on the particles in a fluid motion. The impact of hydro-dynamical forcing on the particles behaviour is examined for different size classes of particles (silt/clay, fine, micro/coarse and macro flocs).

In the first section we present the study area as well as the different measurements and methods used to assess the coupling between turbulence and the particles behaviour over the sea bottom. The meteorological and hydrodynamic contexts occurring during the field measurements are then provided in the next section. The velocity field and the particle size distribution variability are described and their relationships are analysed. The Stokes numbers of these different particles, rarely measured in situ, are also estimated.

2. Data and methods

2.1. Study area

The measurements were conducted in the coastal waters of the eastern English Channel at a fixed station (50°45.676 N, 01°35.117 E) from 25 to 28 June 2012 (Fig. 1A). The different instruments (explained in the data section) are fixed on a structure which was positioned on the seafloor. The English Channel is a mega tidal sea having a tidal range that varies from 3 to 9 m, and experiencing a tidal current of amplitude close to 1.0 m/s (Desprez, 2000; Seuront and Schmitt, 2005; Korotenko et al., 2012). The biogeochemical environment during the particular sampling period is defined from in situ data collected few days before the experiment (21 June) in the frame of the SOMLIT program in two different areas and in high tide period (Fig. 1B). Significant stratification can be noticed from the surface to the bottom at the coastal station for Chlorophyll-a (Chl-a), particulate organic carbon (POC) and suspended particulate matter (SPM) (Table 1). The SPM and Chl-a values are relatively low for a coastal environment, in good agreement with the summer low fresh water discharge, and the absence of phytoplankton bloom. The POC concentration is however relatively high. Besides, the relatively high POC/Chl-a ratio values, a proxy of the carbon mass of living and non-living organisms with respect to the autotrophic organisms (Loisel et al., 2007), indicate that the particulate organic

Table 1
Biogeochemical data collected from SOMLIT few days before the time series measurements (21 June 2012) from the stations C and L (shown in Fig. 1B).

Site	Depth	Temperature (°C)	Salinity (psu)	POC (μg/l)	SPM (mg/l)	Chl-a (μg/l)
C	Surface	15.83	34.43	341.9	NA	0.5
C	Bottom	14.82	34.76	239.67	1.54	0.5
L	Surface	14.88	34.93	220.9	0.48	1.21
L	Bottom	13.92	35.06	85.804	1.63	0.18

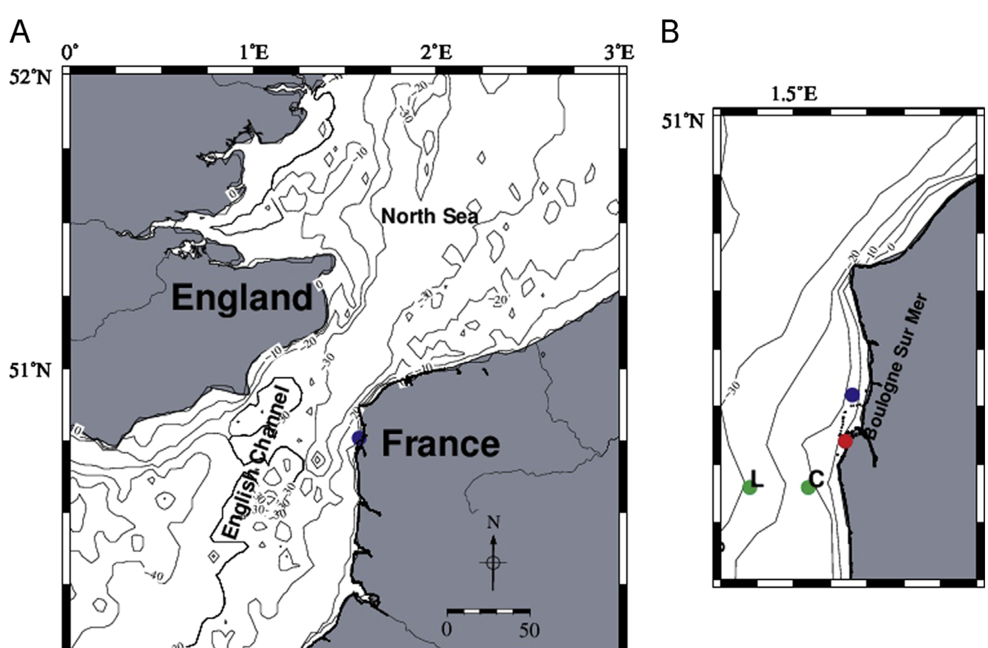

Fig. 1. Location (blue dot) of the sampling area in the eastern English Channel together with the isobaths (A). Zoom on the sampling area (blue dot), the meteorological station (red dot) and SOMLIT stations (green dot) in (B). (For interpretation of the references to colour in this figure caption, the reader is referred to the web version of this paper.)

fraction is largely dominated by detritus and heterotrophic bacteria.

2.2. Data

High frequency time series data were collected at 0.5 m depth above the sea bottom from different instruments fixed on the same platform moored on the sea bed. The three following instruments were used for the present study: a LISST-100x type C (Laser In Situ Scattering and Transmissometry, Sequoia Scientific), a Nortek Vector ADV current meter, and a RDI ADCP. The LISST measures the volume concentration of particles having diameters ranging from 2.5 to 500 μm in 32 size classes in logarithmic scale (Agrawal and Pottsmith, 2000). It also records the beam attenuation (c) at 670 nm (± 0.1 nm) over a 5 cm path length with an acceptance angle of 0.0135°. The particulate beam attenuation coefficient c_p has been derived from c after calibration with MilliQ water before and after the field campaign, using the assumption that chromophoric dissolved organic matter (*CDOM*) does not absorb the light at 670 nm. The volume concentration and c_p are measured with a sampling frequency of 1.0 Hz. The Nortek Vector ADV current meter measured the North, East and up components of the local velocity components with an accuracy of $\pm 0.5\%$ at 1 Hz. The available range of the velocity value measured by the instrument is from 0.01 to 7.0 m/s (± 0.01 m/s). A 1.2 MHz upward-looking four beam broadband RDI ADCP was also deployed on the bottom, along with the previous cited instruments clubbed in a structure. The ADCP was operated in the fast pinging mode, providing two profiles per second. Each velocity was an average of six short pulse measurements over a 2 Hz interval. The velocities were recorded in Cartesian co-ordinates with 0.4 m vertical resolution. The significant wave height *Hs*, peak wave period *Tp*, and peak wave direction *Dp* are derived from the ADCP data using manufacture provided software WavesMon (Teledyne RD Instruments). These wave parameters were computed for 10 min burst duration with a moving window of 5 min interval providing one data point every 5 min. The wind data were provided by the meteorological station of harbour, Boulogne-Sur-Mer light house (*Meteo-France*) with a temporal resolution of 1 h.

2.3. Methods

Particle size distributions and power law of PSD: The scattering patterns of particles at 670 nm are recorded in 32 logarithmically size scattering angles by the LISST-100X type C (Agrawal and Pottsmith, 2000). This instrument measures the volume concentration $C_{vol,i}$ ($\mu l/l$) of the particles in 32 size classes from 2.5 to 500 μm through diffraction technique. Because of instability in the smallest and largest size classes, the data recorded in the first five inner and last outer rigs are excluded from further analysis (Traykovski et al., 1999; Jouon et al., 2008; Reynolds et al., 2010; Neukermans et al., 2012a). These instabilities observed in the smaller size classes have also been related to effects of stray light (Reynolds et al., 2010). Due to multiple scattering effects and signal to noise ratio sensitivity, the data for which optical transmission values are less than 30% and greater than 98% are also disregarded from the statistical analysis (personal communication with Ole Mikkelsen).

The volume concentration distributed on a particle size class can also be expressed as the concentration $C_{vol}(\sigma)$ per unit volume per unit bin width (Jouon et al., 2008):

$$C_{vol}(\sigma) = \frac{C_{vol,i}}{\sigma_{\max}(i) - \sigma_{\min}(i)} \tag{1}$$

where σ is the median diameter of the particle size class i, $\sigma_{\max}(i)$ and $\sigma_{\min}(i)$ are, respectively, the maximum and the minimum particle size of the class i. This resulting volumetric *PSD* is expressed in $\mu l l^{-1} \mu m^{-1}$. The number of particles for a size σ of the *PSD* is estimated by a normalization by their volume (Jouon et al., 2008). We obtain the number density $n(\sigma)$, which is also the product of the probability density function of the size $p(\sigma)$ and the total number of particles N:

$$n(\sigma) = Np(\sigma) = \frac{C_{vol}(\sigma)}{\frac{4}{3}\pi(\sigma/2)^3} \tag{2}$$

The *PSD* of this density number classically follows a power law distribution for aquatic particles in suspension (Sheldon et al., 1972; Kitchen et al., 1982; Jonasz, 1983; Boss et al., 2001a; Twardowski et al., 2001; Loisel et al., 2006; Reynolds et al., 2010):

$$n(\sigma) \sim K\sigma^{-\xi} \tag{3}$$

where K is a constant and ξ is the *PSD* slope. The value of $\xi(t)$ is here estimated at each time step (every second) from the LISST measurements, using an automatic regression analysis. The ξ value provides information on the relative concentration of small and large particles: the steeper the slope (the greater the ξ), the more small particles relative to large particles are present in the water (and vice versa).

Mean particulate diameters: Sauter's diameter (D_A) is the mean diameter of an equivalent sphere which has the same specific surface area as that of the *PSD*. This diameter is commonly used in sedimentology to represent size distribution in fluid flow calculation. Sauter's diameter D_A is also computed from the *PSD* using the following equations (Neukermans et al., 2012a; Filippa et al., 2012):

$$D_A = \frac{\sum_{i=6}^{31} [AC]_i \sigma_i}{[AC]} = \frac{\int_{\sigma_6}^{\sigma_{31}} n(\sigma)\sigma^3 \, d\sigma}{\int_{\sigma_6}^{\sigma_{31}} n(\sigma)\sigma^2 \, d\sigma} = \frac{\int_{\sigma_6}^{\sigma_{31}} p(\sigma)\sigma^3 \, d\sigma}{\int_{\sigma_6}^{\sigma_{31}} p(\sigma)\sigma^2 \, d\sigma} \tag{4}$$

$$[AC]_i = \frac{3}{2\sigma_i} C_{vol}(\sigma) \tag{5}$$

where $[AC]_i$ is the cross sectional area concentration of particles in bin i, and $[AC]$ is the total cross sectional area.

The following size classification has been adopted: silt/clay (<30 μm), fine (<105 μm), coarse/micro (<300 μm) and macrofloc (>300 μm) (Lefebvre et al., 2012). The volume concentration of each size class has been analysed using statistical and dynamical approaches.

Stokes number: In turbulent flows, the largest turbulent eddies break-up into smaller eddies through an energy cascade and finally dissipate at small scale due to molecular viscosity. The size of these smallest eddies is the Kolmogorov length scale. The eddies at this scale have typical life time τ_η which is the smallest time scale of turbulence. The Stokes number St is defined as the non-dimensional ratio of an inertial characteristic time scale τ_p to τ_η. It is one of the fundamental parameters characterizing particle-turbulence interactions: for $St \ll 1$, particles follow passively the fluid flow, whereas for $St \gg 1$, large inertia particles are not influenced by turbulence, and follow their own trajectories. It can also be related to the particles and fluid characteristics (Wang et al., 2000; Schmitt and Seuront, 2008; Xu and Bodenschatz, 2008) as follows:

$$St = \frac{\tau_p}{\tau_\eta} = C_p \left(\frac{\sigma}{\eta}\right)^2 \tag{6}$$

with $C_p = B/18$, where $B = \rho_p/\rho$ is the ratio of the particle density to the fluid density, and $\eta = (\nu^3/\epsilon)^{1/4}$ is the Kolmogorov length scale, where ν and ϵ are the kinematic viscosity of the fluid (in $m^2\,s^{-1}$) and the dissipation rate (in $m^2\,s^{-3}$), respectively.

The value of the dissipation rate ϵ is estimated using the power spectrum of the velocity time series, assuming a local isotropic

Kolmogorov relation of the form (Pope, 2000)

$$E(k) = C\epsilon^{2/3}k^{-5/3} \quad (7)$$

where $E(k)$ is the Fourier power spectrum, $C=1.5$ is a constant and k is the wavenumber. Since the power spectrum is here estimated from a time series in a fixed point, we estimate $E(f)$ where f is the frequency. Frequency and wavenumber are related with the horizontal component of the velocity V: $k=2\pi f/V$. This gives the following estimation of the dissipation from the power spectrum (Sethuraman et al., 1978; Lien and D'Asaro, 2006; Gerbi et al., 2009; Huang et al., 2012; Thomson et al., 2012):

$$\epsilon = \left(\frac{C_0}{C}\right)^{3/2}\left(\frac{2\pi}{\sigma_V}\right)^{5/2} \quad (8)$$

where σ_V is the standard deviation of V and C_0 is the constant such that $E(f)=C_0 f^{-5/3}$ is a best fit estimated over a range of frequencies corresponding to the inertial range.

3. Results

3.1. Meteorological and hydrodynamic conditions

Fig. 2 shows the hydrodynamic conditions prevailing in the study area during the observations. The significant wave height *Hs* exhibits relatively large variability in its magnitude during the entire time series observation (from 0.18 to 0.84 m). The mean and standard deviation values of *Hs* are 0.41 and 0.14 m, respectively. The peak wave period, *Tp*, also presents a relatively great variability from few seconds to 20 s, with a mean and standard deviation values of 6.41 and 2.44 s, respectively. In contrast, the peak wave direction, *Dp*, is almost constant during the entire experiment, with a mean value around 268°, which reveals that the waves are coming from the West. The water level shows typical semi-diurnal tidal characteristics with a period of 12.5 h. The total water column depth observed during the low tide time and the high tide time is 3.74 m and 10.07 m, respectively, revealing the spring tide conditions.

Relatively large wind fluctuations in terms of amplitude and direction are observed during the experiment. Relatively high wind speed values (above 4 m s^{-1}) are generally associated with South West wind (except at the end of the experiment), whereas relatively low wind speeds values (less than 4 m s^{-1}) are generally associated with South East wind.

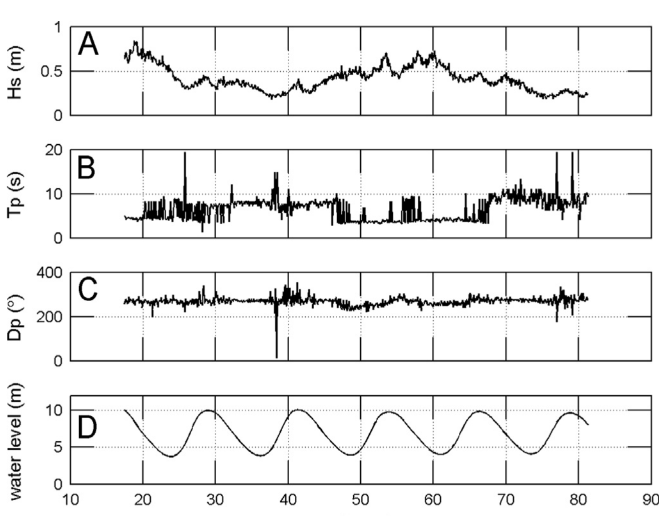

Fig. 2. Time series of (A) the significant wave height *Hs*, (B) peak wave period *Tp*, (C) peak wave direction *Dp*, and (D) water level.

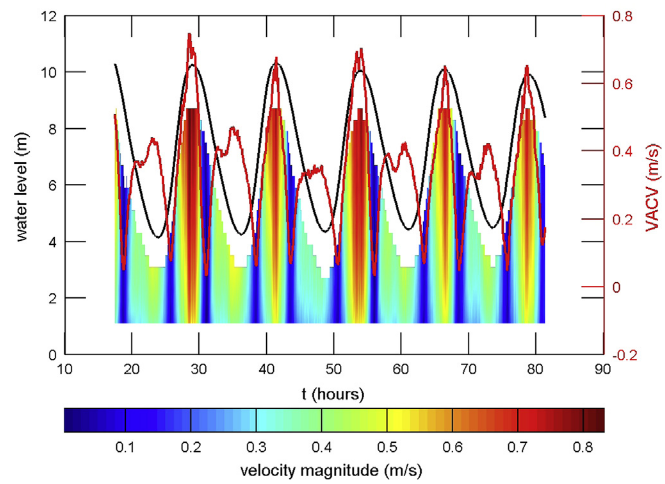

Fig. 3. Time series of water level evolution along with tide (black line), time series of VACV (in red) and contour map showing the vertical structure of the current velocity. (For interpretation of the references to colour in this figure caption, the reader is referred to the web version of this paper.)

From the water level evolution and current data set provided by ADCP, the effect of tidal current on the *PSD* can be analysed. The interval when the speed of the tidal current is very weak or zero usually refers to the period of reversal between ebb and flood currents, and also refers to the slack tide. The vertically averaged current velocity (VACV) has been derived for the entire time series (Fig. 3). VACV shows minimum values during the current reversal time, and two maxima, the main ones corresponding to the high tide (high water), and the second ones, reached at low tide (low water) (Fig. 3). The consecutive intervals of time between flood to ebb and ebb to flood are (7–7.34 h) greater than ebb to flood and flood to ebb (5.1–5.42 h), evidencing a pronounced asymmetry of tidal currents (Fig. 3).

3.2. Stokes number

The estimation of horizontal power spectra (U and V components) was used to estimate the constant C_0 in Eq. (8) and hence the dissipation rate. The mean value of the dissipation rate over the sampling day is $\epsilon = 7.65 \times 10^{-7}$ m^2 s^{-3}. Since the mean temperature value is $T=16.11$ °C (±0.10), the viscosity value is fixed at $\nu = 1.133 \times 10^{-6}$ m^2 s^{-1} (Kestin et al., 1981) and hence the Kolmogorov dissipation length scale $\eta = (\nu^3/\epsilon)^{1/4} = 1.2$ mm. Because the mass density is not measured in the present study, two extreme values are imposed to assess the ratio of the particle density to the fluid density, B. The mass density of mineral and organic particles is $\rho_p = 2.7 \pm 0.15$ g cm^{-3} and $\rho_p = 1.06 \pm 0.03$ g cm^{-3}, respectively (Chiappa-Carrara et al., 2006), resulting in B values of 2.7 ± 0.15 and 1.06 ± 0.03, respectively. Using Eq. (6), these range of values for B, the estimation of ϵ and the range of particle sizes detected by the LISST (6.20–390 μm), we obtain Stokes numbers ranging from 6.8×10^{-7} to 0.03 for mineral particles and from 2.66×10^{-7} to 0.01 for organic particles. The largest values of the Stokes number are found for the largest particles (~0.39 mm), which are still almost four times smaller than the Kolmogorov scale. This shows that the Stokes numbers are here always very small, and that these particles are likely to be passive tracers and move along with the fluids.

3.3. Temporal variability of the velocity field

The time series of along-shore (U) and cross-shore (V) components of the velocity and their corresponding power spectra were estimated using the ADV data (Fig. 4). The along and cross shore

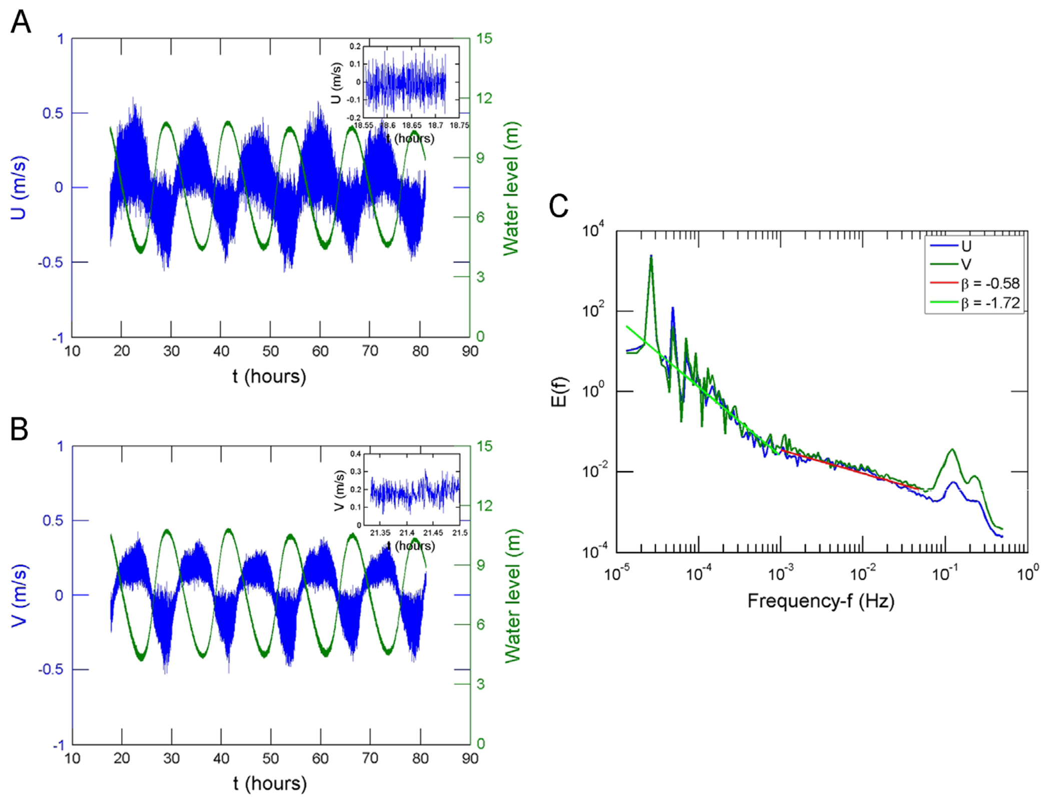

Fig. 4. Time series of U (A) and V (B). The insets represent a small portion of the time series to show the fluctuations. (C) Power spectra of U (blue curve) and V (green curve). The two straight lines correspond to two different scales with slopes of -1.72 (near to $-5/3$ slope of Kolmogorov) in light green and -0.58 in red and the humps in the energy value at high frequency represents a small scale forcing of high energy wave breaking. (For interpretation of the references to colour in this figure caption, the reader is referred to the web version of this paper.)

velocity components are characterized by a periodicity of 12.5 h, and a large small scale variability with a coefficient of variation (i.e., a ratio of standard deviation to the mean value of the absolute velocity also called as turbulent intensity) value for the along-shore and cross-shore components of 64.28 and 50.48%, respectively (Fig. 4A, B). These velocity records are tightly linked to the tidal cycle which also exhibits a period of 12.5 h. The along-shore component is characterized by a higher variability compared to the cross-shore component. The variability patterns of U and V are analysed through their power spectra (Fig. 4C). At low frequency scaling ranges, the power spectra of the two horizontal components (U and V) are characterized by a power law with a slope (β) close to $-5/3$ associated with 3D homogeneous turbulence (Kolmogorov scaling). From $T = 1000\ \mathrm{s} \sim 17$ min there is a transition to a regime for which the power spectra are characterized by a lower slope value (close to -0.6). Similar kind of β value has been observed in the 1-min summer rainfall time series data with a scaling regime from 1 h to 1 day (Yonghe et al., 2013). At high frequencies (0.1–0.3 Hz, hence on the range 3–10 s), the energy spectra exhibit the impact of a localized forcing. Such forcing has previously been attributed to the high energy associated with wave breaking scales (Schmitt et al., 2009).

3.4. *Temporal variability patterns of particles concentration and size parameters in relation with hydrodynamical forcing*

The size parameters considered here are the slope ξ of the *PSD*, as well as D_A and the normalized volume concentration of different size classes (silt/silt, fine, coarse/micro and macro-floc) of aggregates (Lefebvre et al., 2012). The turbidity dynamics is also considered through the particulate attenuation coefficient, $c_p(670)$, which is proportional to the particle concentration, at first order (Neukermans et al., 2012b). The number of particles in size class i per unit volume and per unit diameter increment $n(\sigma)$ is computed for the entire size classes at each time step (Fig. 5). The *PSD* of the present data set is well represented by a power-law distribution throughout the whole time series. The slope values, ξ, of the particulate size distribution range between 2.57 and 3.94, with a mean value of 2.9 and a standard deviation of 0.16. These values are in good agreement with previous studies (Jonasz, 1983; Boss et al., 2001b; Loisel et al., 2006; Buonassissi and Dierssen, 2010; Reynolds et al., 2010; Neukermans et al., 2012a).

The Probability Density Function (*PDF*) of the concentrations and size parameters followed non-Gaussian distributions (Fig. 6). The inset of each panel in Fig. 6 shows the *PDF* and the Gaussian fit in a semi-log scale in order to emphasize extreme values. All the parameters show an asymmetry, and some are showing a heavy tail in their distribution (Fig. 6C–E). In addition, chi-square goodness-of-fit tests have been performed to test the normal distribution; the test result rejects the null hypothesis that these parameters come from a normal distribution with a mean and a variance computed from these parameters, at 5% significance level with a p-value of 0 and $h = 1$.

The temporal variability of $\xi(t)$ is analysed along with the vertically averaged current velocity (VACV) showing the tidal information as well as the current reversal (Fig. 7A). At the time of the current reversal, that is when VACV is minimum, $\xi(t)$ generally exhibits a well pronounced peak. This pattern indicates that the proportion of small particles compared to larger ones increases at this particular time. The mean diameter D_A, estimated for each time step, exhibits strong high frequency variability and has a mean value of 116.57 μm and standard deviation of ± 20.43 μm (Fig. 7B). D_A presents a well pronounced trough in

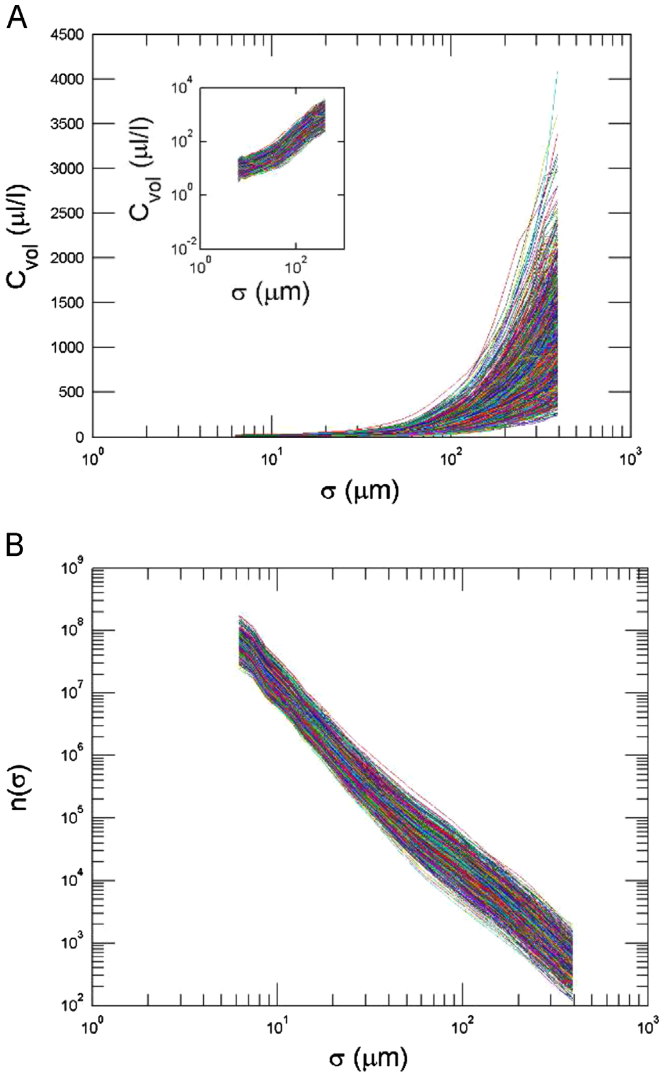

Fig. 5. *PSD* for volume concentration (A) and for number concentration (B). The inset in (A) is a log–log plot emphasizing the power-law relations for the volume concentrations.

magnitude during the current reversal time in agreement with the $\xi(t)$ patterns. This impact of current reversal on particles size distribution is also well evidenced through the temporal evolution of the normalized volume concentration of each considered size class (Fig. 7D–G). During slack tide the normalized volume concentration presents relatively higher values (a peak) in the lower size classes (silt/clay and fine) (Fig. 7D, E) and lower values (a trough) in the complementary higher size classes (coarse/micro and macro-flocs) (Fig. 7F, G). The time series of $c_p(670)$, a proxy of the suspended particulate concentration, exhibits strong high frequency variability (coefficient of variation of 53%), with numerous peaks which generally occur when the VACV is maximum (Fig. 7C). The mean and the standard deviation of $c_p(670)$ are 10.38 and 5.53 m^{-1}, respectively.

Besides the apparent impact of the vertically averaged current velocity on the particles concentration and size distribution, the significant wave height also slightly contributes to the re-suspension effects ($r^2 = 0.23$). The larger the mean significant wave height, the more the concentration of re-suspended particles (Fig. 8A). Moreover, significant wave height seems to affect *PSD* by promoting the concentration of larger particles compared to smaller ones (Fig. 8B). However, according to the low determination coefficient value additional data are needed to confirm this last point.

Since we have high frequency time series of $\xi(t)$, $D_A(t)$, $c_p(670)(t)$ and normalized volume concentration of each size classes of particles, we can explore their dynamical properties. The dynamics of ξ, D_A and $c_p(670)$ has been estimated through power spectral analysis (Fig. 9A–C). Two scaling regimes characterized by different slope values are observed on either side of the period of $T = 1000$ s, similar to the velocity period. These parameters in the low frequency regime present the same spectral slope (β close to $-5/3$) similar to the velocity field, indicating that the dynamics of the particles is influenced by turbulence at low frequencies. At higher frequencies, the slope values of these parameters and velocity field are significantly different but remain similar to the velocity spectra. With a slope value close to -0.8 in the frequency range $[0.001; 0.1\ \mathrm{s}^{-1}]$, the dynamics of the particles seems to be partly driven by dynamical processes likely impacted by the interaction with the sea floor for which a slope of -1.0 is expected (Perry et al., 1986; Katul et al., 1995; Katul and Chu, 1998). Similar power spectra are also observed in the case of normalized volume concentrations of different size classes of particles (Fig. 9D).

4. Discussion and conclusion

Large temporal variability in the hydrodynamic fields, particle concentration and size distribution was observed during the in situ experiment reported here. The hydrodynamic conditions, along with the high turbulence level encountered, provide favourable conditions for the re-suspension of particle. The present data set has shown that tidal current and waves have a significant role in the particle re-suspension and further water column turbidity. This is in good agreement with Velegrakis et al. (1999) who observed large scale particle re-suspension processes generated by the tidal current and coastal waves for the same region. During the current reversal, when the VACV is minimum, all the size parameters examined here indicate a modification in the particle size distribution. The proportions of small particles tend to increase compared to bigger ones (Fig. 7). Two processes can explain this pattern. First, hydrodynamic forcing is not sufficient to re-suspend large particulate assemblages from the bottom. Second, during the period of slack current, the differential settling of particles one over the other takes place inducing a washing of the water column, especially of heavy flocs. These observations agree with the study carried out by Van Leussen (1988). To a lesser extent, the occurrence of waves induces an increase of the suspended particulate matter concentration (i.e. $c_p(670)$), and especially of large particulate assemble (Fig. 8).

Turbulence has been extracted from the along shore and cross-shore components of the current velocity, which show periodic fluctuations in their magnitude. The power spectra of velocity components follow three different regimes depending on the scale. The first one, with typical inertial range, has a slope close to $-5/3$. The second one is characterized by a flatter slope of -0.6 with a transition scale of 1000 s. At last, the energy spectra at high frequencies (3–10 s) show a localized forcing attributed to waves forcing, similar to the previous results obtained in the same region (Schmitt et al., 2009). From $T = 1000\ \mathrm{s} \sim 17$ min there is a transition to a regime for which the power spectra are characterized by a lower slope value (close to -0.6). While there is still no theoretical explanation of such low slope value, theoretical studies have shown that the power spectra of velocities close to the sea floor may be characterized by a slope value of -1.0 (Panchev, 1971; Kader and Yaglom, 1984; Katul and Chu, 1998). The theoretical and experimental studies carried out by Perry et al. (1986), Katul et al. (1995), and Katul and Chu (1998) showed that the

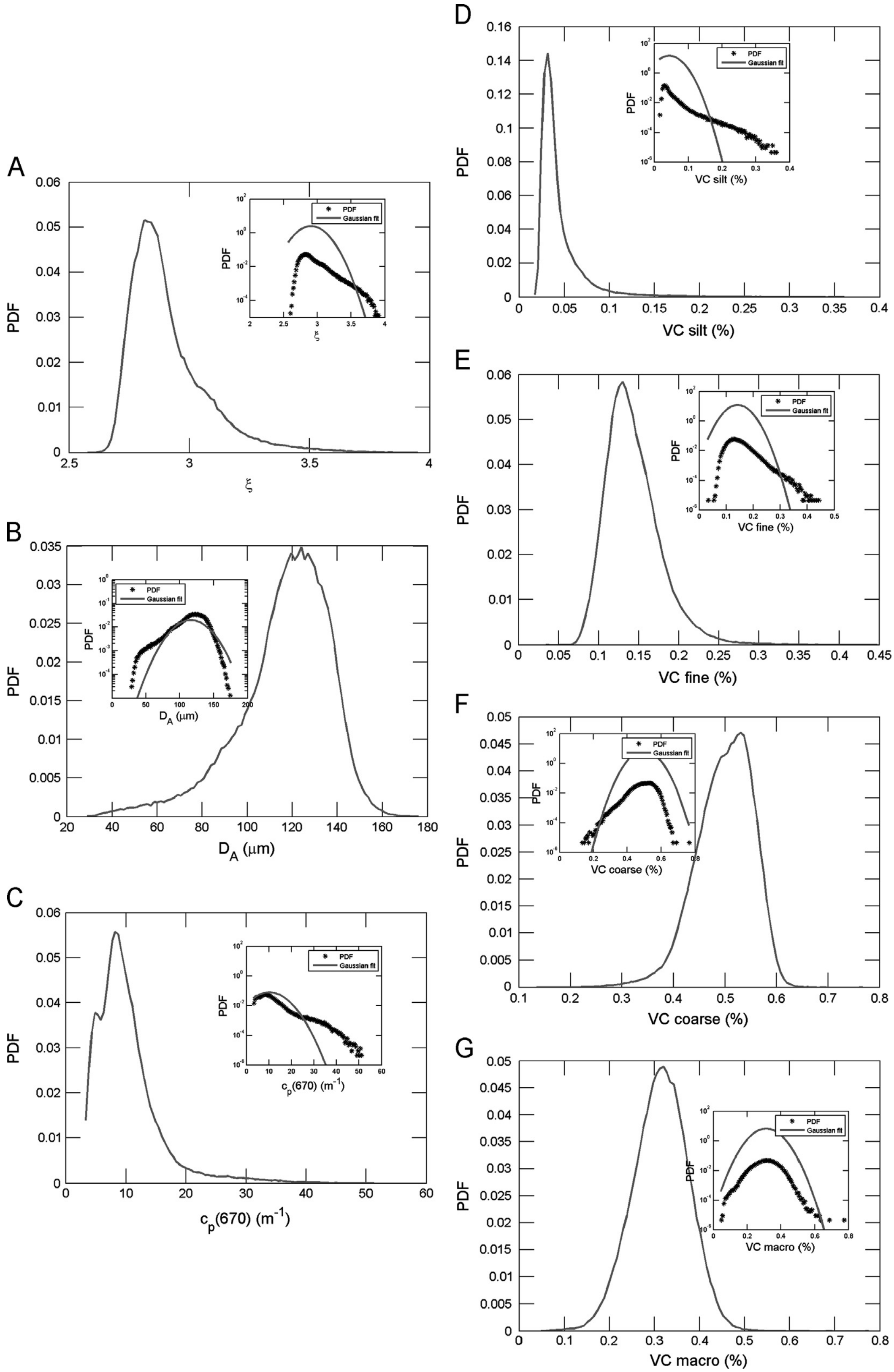

Fig. 6. The *PDF* of (A) ξ, (B) D_A, (C) $c_p(670)$ and normalized volume concentration of the different size classes of particles (*VC silt* (D), *VC fine* (E), *VC coarse* (F) and *VC macro* (G)), superposed to a Gaussian fit with the same mean and variance. The inset in all figures is a semi-log plot emphasizing extremes, showing that all *PDF*s are non-Gaussian.

turbulent boundary layer was characterized by a power-spectral slope of -1.0 at the low wave number values.

Thus, the power spectra of size parameters and $c_p(670)$ exhibit very similar turbulent scaling in the lower and higher frequency regions compared to the velocity field. The Stokes number derived from the present measurements exhibits very low values ($\ll 1$), showing that the particles in the fluid motion behave like tracers and move along with the fluid.

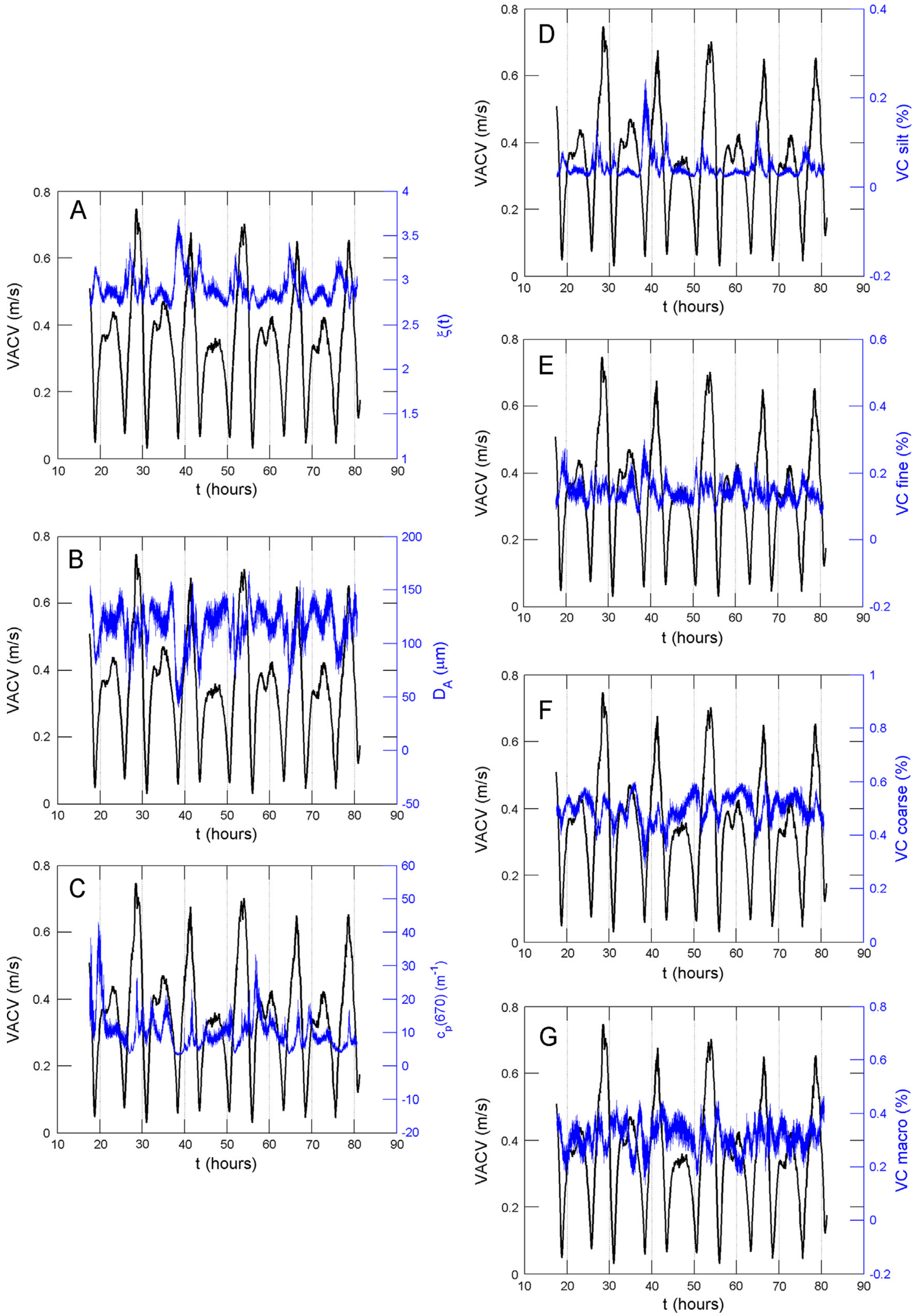

Fig. 7. Time series of (A) $\xi(t)$, (B) D_A, (C) $c_p(670)$ and the normalized volume concentration of different size classes of particles (*VC silt* (D), *VC fine* (E), *VC coarse* (F) and *VC macro* (G)) superposed to VACV data.

We found that turbulence has a great role in the dynamics of the particles in the present region. Low frequency variability of the particles is controlled by the turbulence ($\beta \simeq -5/3$) and high frequency variability is controlled by the physical processes which are related to the sea bottom interactions (wall turbulence), tidal currents and waves. A next step related to this work will be to analyze the turbulent intermittency scaling of these parameters using empirical mode decomposition (Huang et al., 2008). Other

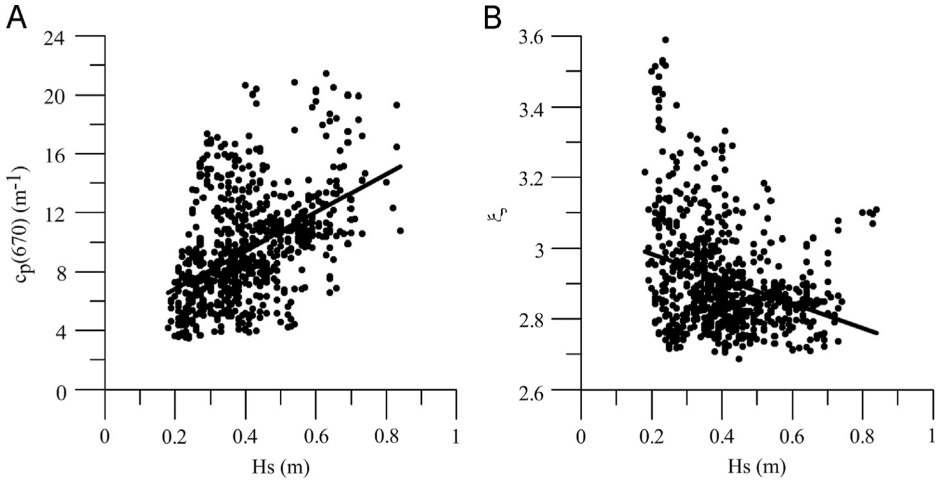

Fig. 8. (A) Scatter plot of $c_p(670)$ versus *Hs* and (B) ξ versus *Hs*.

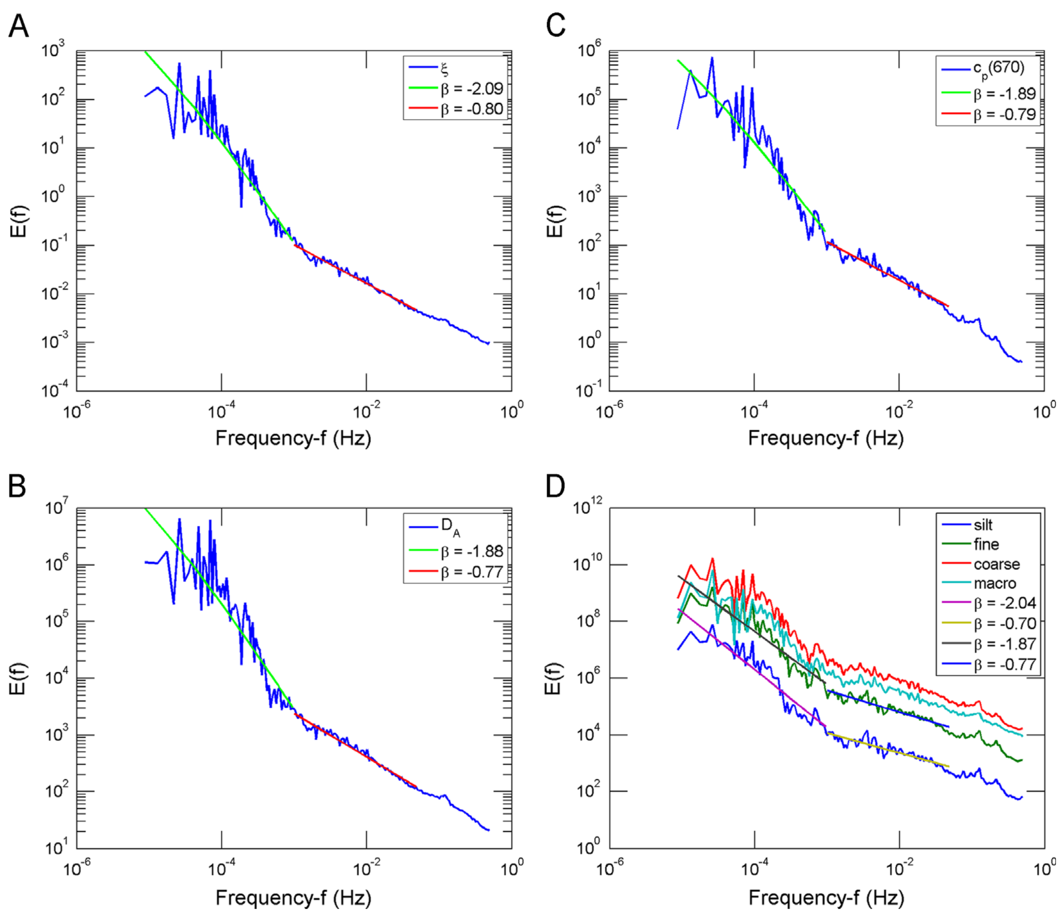

Fig. 9. Power spectra of ξ, D_A, $c_p(670)$ and the total volume concentrations of different size classes of particles showing different scale regimes as indicated by the different slope values for different frequency ranges.

measurement campaigns will be performed in coastal waters to compare with the present study and assess its possible universality.

Acknowledgements

Centre National d'Etudes Spatiales (CNES) and Centre National de la Recherche Scientifique (CNRS) are acknowledged for the funding of P.R. Renosh's Ph.D thesis. Meteo France is acknowledged for providing wind data. The biogeochemical data were provided by Service d'Observation en Milieu Littoral, INSU-CNRS, Wimereux. This study is performed in the frame of the COULCOT-2 project, funded by the CNES/TOSCA program.

References

Agrawal, Y.C., Pottsmith, H.C., 2000. Instruments for particle size and settling velocity observations in sediment transport. Mar. Geol. 168, 89–114.

Berhane, I., Sternberg, R.W., Kineke, G.C., Milligan, T.G., Kranck, K., 1997. The variability of suspended aggregates on the Amazon Continental Shelf. Cont. Shelf Res. 17, 267–285.

Boss, E., Pegau, W.S., Gardner, W.D., Zaneveld, J.R.V., Barnard, A.H., Twardowski, M.S., Dickey, T.D., 2001a. Spectral particulate attenuation and particle size distribution in the bottom boundary layer of a continental shelf. J. Geophys. Res. 106 (C5), 9509–9516.

Boss, E., Twardowski, M.S., Herring, S., 2001b. Shape of the particulate beam attenuation spectrum and its inversion to obtain the shape of the particulate size distribution. Appl. Opt. 40, 4885–4893.

Boss, E., Slade, W., Hill, P., 2009. Effect of particulate aggregation in aquatic environments on the beam attenuation and its utility as a proxy for particulate mass. Opt. Express 17, 9408–9420.

Buonassissi, C.J., Dierssen, H.M., 2010. A regional comparison of particle size distributions and the power law approximation in oceanic and estuarine surface waters. J. Geophys. Res. 115, C10028.

Burchard, H., Craig, P.D., Gemmrich, J.R., van Haren, H., Mathieu, P.P., Meier, H.E., Wijesekera, H.W., 2008. Observational and numerical modeling methods for quantifying coastal ocean turbulence and mixing. Prog. Oceanogr. 76, 399–442.

Chiappa-Carrara, X., Rioja-Nieto, R., Mascaro, M., 2006. Mass density assessment: comparison of three methods using *Oikopleura dioica* (Appendicularia) as a model system. Carribean J. Sci. 42, 231–238.

Desprez, M., 2000. Physical and biological impact of marine aggregate extraction along the French coast of the Eastern English Channel: short- and long-term post-dredging restoration. ICES J. Mar. Sci. 57, 1428–1438.

Eisma, D., 1986. Flocculation and de-flocculation of suspended matter in estuaries. Neth. J. Sea Res. 20, 183–199.

Fettweis, M., Francken, F., Pison, V., Van den Eynde, D., 2006. Suspended particulate matter dynamics and aggregate sizes in a high turbidity area. Mar. Geol. 235, 63–74.

Filippa, L., Trento, A., Alvarez, A.M., 2012. Sauter mean diameter determination for the fine fraction of suspended sediments using a LISST-25X diffractometer. Measurement 45, 364–368.

Fowler, S.W., Knauer, G.A., 1986. Role of large particles in the transport of elements and organic compounds through the oceanic water column. Prog. Oceanogr. 16, 147–194.

Gerbi, G.P., Trowbridge, J.H., Terray, E.A., Plueddemann, A.J., Kukulka, T., 2009. Observations of turbulence in the ocean surface boundary layer: energetics and transport. J. Phys. Oceanogr. 39, 1077–1096.

Hill, P.S., 1998. Controls on floc size in the sea. Oceanography 11, 13–18.

Huang, Z.C., Lenain, L., Melville, W.K., Middleton, J.H., Reineman, B., Statom, N., McCabe, R.M., 2012. Dissipation of wave energy and turbulence in a shallow coral reef lagoon. J. Geophys. Res. 117, C03015.

Huang, Y.X., Schmitt, F.G., Lu, Z.M., Liu, Y.L., 2008. An amplitude-frequency study of turbulent scaling intermittency using empirical mode decomposition and Hilbert spectral analysis. EPL 84, 40010.

Jonasz, M., 1983. Particle-size distributions in the Baltic. Tellus B 35, 346–358.

Jouon, A., Ouillon, S., Douillet, P., Lefebvre, J.P., Fernandez, J.M., Mari, X., Froidefond, J.M., 2008. Spatio-temporal variability in suspended particulate matter concentration and the role of aggregation on size distribution in a coral reef lagoon. Mar. Geol. 256, 36–48.

Kader, B.A., Yaglom, A.M., 1984. Turbulent structure of an unstable atmospheric layer. In: Sagdeyev, R.Z. (Ed.), Nonlinear and Turbulent Processes in Physics, vol. 2. Harwood Academic, Boston, pp. 829–845.

Katul, G., Chu, C.R., 1998. A Theoretical and experimental investigation of energy-containing scales in the dynamic sublayer of boundary-layer flows. Boundary-Layer Meteorol. 86, 279–312.

Katul, G.G., Chu, C.R., Parlange, M.B., Albertson, J.D., Ortenburger, T.A., 1995. Low-wavenumber spectral characteristics of velocity and temperature in the atmospheric surface layer. J. Geophys. Res. 100 (D7), 14243–14255.

Kestin, J., Khalifa, H.E., Correia, R.J., 1981. Tables of the dynamic and kinematic viscosity of aqueous NaCl solutions in the temperature range 20–150 °C and the pressure range 0.1–35 MPa. Am. Chem. Soc. Amer. Inst. Phys. Natl. Bur. Stand. 10, 71–87.

Kitchen, J.C., Zaneveld, J.R.V., Pak, H., 1982. Effect of particle size distribution and chlorophyll content on beam attenuation spectra. Appl. Opt. 21, 3913–3918.

Korotenko, K.A., Sentchev, A.V., Schmitt, F.G., 2012. Effect of variable winds on current structure and Reynolds stresses in a tidal flow: analysis of experimental data in the eastern English Channel. Ocean Sci. 8, 1025–1040.

Kranck, K., Milligan, T.G., 1992. Characteristics of suspended particles at an 11 hour anchor station in San Francisco Bay, California. J. Geophys. Res. 97 (C7), 11373–11382.

Lefebvre, J.P., Ouillon, S., Vinh, V.D., Arfi, R., Panché, J.Y., Mari, X., Torréton, J.P., 2012. Seasonal variability of cohesive sediment aggregation in the Bach Dang-Cam Estuary, Haiphong (Vietnam). Geo-Mar. Lett. 32, 103–121.

Lien, R.C., D'Asaro, E.A., 2006. Measurement of turbulent kinetic energy dissipation rate with a Lagrangian float. J. Atmos. Ocean. Technol. 23, 964–976.

Loisel, H., Mériaux, X., Berthon, J.F., Poteau, A., 2007. Investigation of the optical backscattering to scattering ratio of marine particles in relation to their biogeochemical composition in the eastern English Channel and southern North Sea. Limnol. Oceanogr. 52, 739–752.

Loisel, H., Nicolas, J.M., Sciandra, A., Stramski, D., Poteau, A., 2006. Spectral dependency of optical backscattering by marine particles from satellite remote sensing of the global ocean. J. Geophys. Res. 111, C09024.

McCave, I.N., 1984. Size spectra and aggregation of suspended particles in the deep ocean. Deep Sea Res. A. Oceanogr. Res. Pap. 31, 329–352.

Mikkelsen, O., Pejrup, M., 2001. The use of a LISST-100 laser particle sizer for in-situ estimates of floc size, density and settling velocity. Geo-Mar. Lett. 20, 187–195.

Neukermans, G., Loisel, H., Mériaux, X., Astoreca, R., McKee, D., 2012a. In situ variability of mass-specific beam attenuation and backscattering of marine particles with respect to particle size, density, and composition. Limnol Oceanogr. 57, 124–144.

Neukermans, G., Ruddick, K., Loisel, H., Roose, P., 2012b. Optimization and quality control of suspended particulate matter concentration measurement using turbidity measurements. Limnol. Oceanogr.: Methods 10, 1011–1023.

Panchev, S., 1971. Random Functions and Turbulence. Pergamon Press, Oxford p. 443

Perry, A.E., Henbest, S., Chong, M.S., 1986. A theoretical and experimental study of wall turbulence. J. Fluid Mech. 165, 163–199.

Pope, S.B., 2000. Turbulent Flows. Cambridge University Press, Cambridge p. 770

Reynolds, R.A., Stramski, D., Wright, V.M., Wozniak, S.B., 2010. Measurements and characterization of particle size distributions in coastal waters. J. Geophys. Res. 115, C08024.

Schmitt, F.G., Huang, Y., Lu, Z., Liu, Y., Fernandez, N., 2009. Analysis of velocity fluctuations and their intermittency properties in the surf zone using empirical mode decomposition. J. Mar. Syst. 77, 473–481.

Schmitt, F.G., Seuront, L., 2008. Intermittent turbulence and copepod dynamics: increase in encounter rates through preferential concentration. J. Mar. Syst. 70, 263–272.

Sethuraman, S., Meyers, R.E., Brown, R.M., 1978. A comparison of a Eulerian and a Lagrangian time scale for over-water atmospheric flows during stable conditions. Boundary-Layer Meteorol. 14, 557–565.

Seuront, L., Schmitt, F.G., 2005. Multiscaling statistical procedures for the exploration of biophysical couplings in intermittent turbulence. Part II. Applications. Deep Sea Res. II 52, 1325–1343.

Sheldon, R.W., Prakash, A., Sutcliffe , W.H., 1972. The size distribution of particles in the ocean. Limnol. Oceanogr. 17, 327–340.

Stramski, D., Boss, E., Bogucki, D., Voss, K.J., 2004. The role of seawater constituents in light backscattering in the ocean. Prog. Oceanogr. 61, 27–56.

Thomson, J., Polagye, B., Durgesh, V., Richmond, M.C., 2012. Measurements of turbulence at two tidal energy sites in Puget Sound, WA. IEEE J. Ocean. Eng. 37, 363–374.

Traykovski, P., Latter, R.J., Irish, J.D., 1999. A laboratory evaluation of the laser in situ scattering and transmissometery instrument using natural sediments. Mar. Geol. 159, 355–367.

Twardowski, M.S., Boss, E., Macdonald, J.B., Pegau, W.S., Barnard, A.H., Zaneveld, J.R.V., 2001. A model for estimating bulk refractive index from the optical backscattering ratio and the implications for understanding particle composition in case I and case II waters. J. Geophys. Res: Oceans 106 (C7), 14129–14142.

Umlauf, L., Burchard, H., 2005. Second-order turbulence closure models for geophysical boundary layers. A review of recent work. Cont. Shelf Res. 25, 795–827.

Van der Lee, E.M., Bowers, D.G., Kyte, E., 2009. Remote sensing of temporal and spatial patterns of suspended particle size in the Irish Sea in relation to the Kolmogorov microscale. Cont. Shelf Res. 29, 1213–1225.

Van Leussen, W., 1988. Aggregation of particles, settling velocity of mud flocs a review. In: Dronkers, J., Van Leussen, W. (Eds.), Physical Processes in Estuaries. Springer, Berlin, Heidelberg, pp. 347–403.

Vantrepotte, V., Brunet, C., Mériaux, X., Lécuyer, E., Vellucci, V., Santer, R., 2007. Bio-optical properties of coastal waters in the Eastern English Channel. Estuar. Coast. Shelf Sci. 72, 201–212.

Velegrakis, A.F., Michel, D., Collins, M.B., Lafite, R., Oikonomou, E.K., Dupont, J.P., Bishop, C., 1999. Sources, sinks and resuspension of suspended particulate matter in the eastern English Channel. Cont. Shelf Res. 19, 1933–1957.

Wang, L.P., Wexler, A.S., Zhou, Y., 2000. Statistical mechanical description and modelling of turbulent collision of inertial particles. J. Fluid Mech. 415, 117–153.

Wells, M.L., Goldberg, E.D., 1992. Marine submicron particles. Mar. Chem. 40, 5–18.

Wolanski, E., Gibbs, R.J., 1995. Flocculation of suspended sediment in the Fly River estuary, Papua New Guinea. J. Coast. Res. 11, 754–762.

Xu, H., Bodenschatz, E., 2008. Motion of inertial particles with size larger than Kolmogorov scale in turbulent flows. Physica D 237, 2095–2100.

Yonghe, L., Kexin, Z., Wanchang, Z., Yuehong, S., Hongqin, P., Jinming, F., 2013. Multifractal analysis of 1-min summer rainfall time series from a monsoonal watershed in eastern China. Theor. Appl. Climatol. 111 (1–2), 37–50.